Available online at www.sciencedirect.com

ScienceDirect

Journal of Nutritional Biochemistry 133 (2024) 109708

Journal of Nutritional Biochemistry

RESEARCH PAPER

The attenuation of gut microbiota-derived short-chain fatty acids elevates lipid transportation through suppression of the intestinal HDAC3-H3K27ac-PPAR-γ axis in gestational diabetes mellitus

Hao Chen[a,b,c,#], Shi-Han Wang[a,b,d,#], Hong-Li Li[a,b,#], Xiao-Bo Zhou[a,b], Lin-Wei Zhou[a,b], Chang Chen[a,b,e], Toby Mansell[g], Boris Novakovic[g], Richard Saffery[g], Philip N. Baker[b,h], Ting-Li Han[f,**], Hua Zhang[a,b,*]

[a] Department of Obstetrics and Gynecology, The First Affiliated Hospital of Chongqing Medical University, Chongqing, China
[b] Canada-China-New Zealand Joint Laboratory of Maternal and Fetal Medicine, Chongqing Medical University, Chongqing, China
[c] Reproductive Medicine Center, Department of Obstetrics and Gynecology, The Affiliated Hospital of Guizhou Medical University, Guiyang, Guizhou, 550009, China
[d] Department of Obstetrics and Gynecology, Daping Hospital, Army Medical University (Third Military Medical University), Chongqing, China
[e] Institute of Life Sciences, Chongqing Medical University, Chongqing, China
[f] Department of Obstetrics and Gynecology, The Second Affiliated Hospital of Chongqing Medical University, Chongqing, China
[g] Murdoch Children's Research Institute and Department of Paediatrics, University of Melbourne, Melbourne, Victoria, Australia
[h] College of Life Sciences, University of Leicester, Great Britain, UK

Received 17 October 2023; received in revised form 20 July 2024; accepted 22 July 2024

Abstract

Gut flora is considered to modulate lipid transport from the intestine into the bloodstream, and thus may potentially participate in the development of GDM. Although previous studies have shown that the intestinal microbiota influences lipid transport and metabolism in GDM, the precise mechanisms remain elusive. To address this, we used a high-fat diet (HFD)-induced GDM mouse model and conducted 16s rRNA sequencing and fecal metabolomics to assess gut microbial community shifts and associated metabolite changes. Western blot, ELISA, and chromatin immunoprecipitation (ChIP) were utilized to elucidate how gut microbiota affect intestinal lipid transport and the insulin sensitivity of hepatic, adipose, and skeletal muscle tissues. We found that HFD impaired the oral glucose tolerance test (OGTT) and insulin tolerance test (ITT) in pregnant mice. 16s rRNA sequencing demonstrated profound compositional changes, especially in the relative abundances of *Firmicutes* and *Bacteroidetes*. Metabolomics analysis presented a decline in the concentration of short-chain fatty acids (SCFAs) in the GDM group. Western blot analyses showed an upregulation of HDAC3 and a concurrent reduction in H3K27 acetylation in the intestine. ChIP-qPCR showed that PPAR-γ was inhibited, which in turn activated lipid-transporter CD36. ELISA and insulin signaling pathway detection in insulin-target organs showed high concentrations of circulating fatty acids and triglycerides and insulin resistance in insulin-target organs. Our results suggest that gut microbiota is closely associated with the development of GDM, partly because decreased gut flora-associated SCFAs activate CD36 by suppressing the HDAC3-H3K27ac-PPAR-γ axis to transport excessive fatty acids and triglycerides into blood circulation, thereby dysregulating the insulin sensitivity of insulin target organs.

Keywords: CD36; GDM; Gut microbiota; H3K27ac; Insulin resistance; SCFA.

1. Introduction

Gestational diabetes mellitus (GDM) is one of the most common pregnancy complications, characterized by insufficient insulin secretion elevated insulin resistance, and generally affects 5–20% of pregnant women [1]. Physiological adaptations to pregnancy include increased insulin resistance and elevated free fatty acids [2,3]. Aberrant insulin sensitivity in peripheral target organs such as liver, muscle, and adipose tissue leads to insulin secretion decompensation, disordered glucose metabolism, and the development of GDM. Changes in daily dietary composition that may be accompanied by unhealthy lifestyles, including a high-fat diet, over-nutrition, and sedentary behavior, exacerbate the likelihood of pregnant women suffering from GDM [1]. GDM increases perinatal morbidity and the risk of maternal type two diabetes mellitus after pregnancy, amongst several adverse health impacts for mothers and their offspring [4].

* Corresponding author at: Chongqing, China 400016.
** Corresponding author at: Chongqing, China 400010.
E-mail addresses: t.han@auckland.ac.nz (T.-L. Han), zh2844@gmail.com (H. Zhang).
Joint first authors.

https://doi.org/10.1016/j.jnutbio.2024.109708

Recently, many studies have shown that the gut microbiota influences the occurrence and development of GDM. Intestinal microbiome homeostasis plays a key role in the regulation of insulin resistance in patients with type two diabetes mellitus and GDM [5,6]. Dysbiosis caused by the modern high-fat diet is closely related to changes in glucose homeostasis and insulin sensitivity [7], and the ecological imbalance of the intestinal microbiome affects the occurrence of metabolic diseases such as obesity, type two diabetes mellitus, and GDM [6,8]. There are diverse microorganisms in our gut, of which the density of bacteria in the colon reaches about 10^{12}/ml [9]. The flora planting in the human gut are mainly divided into five bacterial phylums: *Firmicutes* (60–80%), *Bacteroides* (15–25%), *Proteobacteria* (1–10%), *Actinomycetes* (2.5-5%), and *Verrucomicrophyla* (0.1–2.2%) [10]. They play a crucial role in many physiologic and metabolic processes of our body, including the synthesis of vitamins and nutrients, regulation of metabolism, and development of the immune system [11]. The constitution of the gut microbiome can be regulated by a combination of factors, including the diet, age, and gestation of the host. Notably, the gut microbial ecosystem changes under the influence of a high-fat diet during pregnancy, decreasing the number of gram-negative bacteria and probiotics [12]. This intestinal dysbiosis seems to reduce the production of short-chain fatty acids (SCFAs) and increases susceptibility to GDM [13–15].

SCFAs are a class of fatty acids with less than six carbon atoms, including formic acid, acetic acid, propionic acid, butyric acid, and valeric acid. They act as the main metabolites of the intestinal microbiome, primarily produced by the fermentation of undigested carbohydrate-food cellulose through anaerobic bacteria in the intestine. The types and quantities of SCFAs in the intestine are heavily influenced by bacterial species and substrates (derived from food) [16]. SCFAs potentially regulate host metabolism and improve glucose homeostasis by increasing energy expenditure and ameliorating insulin sensitivity [17,18]. SCFAs inhibit histone deacetylase 3 (HDAC3); without SCFAs, HDAC3 promotes the absorption and transport of fatty acids in the intestine [16]. HDAC3 induces the deacetylation of histone three at lysine 27 (H3K27), thus playing a role in chromatin accessibility and relevant gene transcription regulation [19]. Moreover, there is evidence that H3K27ac promotes PPAR-γ expression [20,21], and that there are interactions between PPARs and the gut microbiota. PPARs are activated by bacteria and regulate the composition of the microbiome [22]. Butyrate is one of the SCFAs known to activate PPAR-γ [23,24], which negatively regulates the expression of CD36 and further promotes lipid uptake and transport in the intestine [25]. Although many studies highlight the role of gut microbiota in the development of GDM, the underlying mechanisms remain unknown.

Therefore, this study used a high-fat diet mouse model of GDM to analyze the relationship between the intestinal microbiome and GDM. We further explored the potential molecular mechanism of elevated insulin resistance in peripheral insulin target organs through abnormal free fatty acids in blood circulation caused by intestinal dysbiosis, reduced SCFAs, and increased lipid metabolism and transport. Thus, our study may enhance the understanding of the pathogenesis of GDM and provide a theoretical basis for formulating novel strategical targets for the SCFA-produced gut microbiota.

2. Materials and methods

2.1. Human subjects

Fecal samples from humans were collected from the Department of Obstetrics at the First Affiliated Hospital of Chongqing Medical University, China, and approved by the Ethics Committee of Chongqing Medical University (2024-062-02). The criteria for fecal samples were as follows: (1) prior to sample collection, no antibiotic treatment within 7 days; (2) no lactic acid products supplement within 5 days. (3) overnight fasting. Fecal donors or the mice fecal microbiota transplantation (FMT) were from 3 GDM pregnant women who were diagnosed by the International Association of the Diabetes and Pregnancy Study Groups (IADPSG) criteria [26], and 3 normoglycemic pregnant women. Each fecal sample was resuspended in PBS, followed by a centrifuge to obtain the supernatant [27].

2.2. Mouse model building

C57BL/6J mice were from the Experimental Animal Center of Chongqing Medical University, weighing 18–19 g, and approved by the Ethics Committee of Chongqing Medical University (2020–568). All animals were bred under specific pathogen-free (SPF) conditions with a normal diet. Mice were housed at five animals per cage in a 12-h light/12-h dark cycle with ad libitum access to food and water at a controlled temperature (23°C±2°C). All animal protocols in this study were approved by the Committee of Institutional Animal Care and Research. After all female mice were fed with ordinary feed until their body weight reached 20g, they were randomly divided into two groups: the NC group (n=15) and the GDM group (n=15). The GDM group was fed a high-fat diet (HFD) with 60% kcal from fat (D12492, Research Diets Inc.) for one week, and the NC group was fed a normal diet for one week. Then they were mated with the male mice in a cage with a ratio of 2:1. The occurrence of vaginal tamponade in the next morning was considered to be day 0.5 of pregnancy. After confirmation of pregnancy, the GDM group kept feeding with an HFD, and the normal control (NC) group was fed with a normal diet. For the FMT mice model, mice were transplanted with fecal supernatant from GDM women (GDM-FMT group), normoglycemic pregnant women (Normal-FMT group), and PBS (Control-FMT group), respectively. All the FMT mice were given a 5 days antibiotic therapy (vancomycin, 100 mg/kg; neomycin sulfate, metronidazole, and ampicillin, 200 mg/kg) before FMT treatment [28]. Subsequently, each mouse was gavaged with 100 μL of prepared fecal supernatant or PBS twice a week for 5 weeks. At gestational day 16.5, mice were euthanized via eyeball blood extirpating, and tissue samples were collected. The success of the GDM model was defined by HOMA-IR.

2.3. Oral glucose tolerance test (OGTT) and insulin tolerance test (ITT)

The mice were fasted for 6 h before each OGTT. Glucose (2 g/kg body weight) was given by oral gavage. Tail vein blood samples were obtained to measure glucose levels at 0, 30, 60, 90, and 120 minutes after glucose gavage, and then the oral glucose tolerance curve was plotted. The area under the curve was calculated and the differences between the groups were compared. OGTTs were performed on gestational days 0.5, 11.5, and 16.5, corresponding to the first trimester, the second trimester, and the third trimester. Insulin solution was administered at a dose of 0.5 IU/kg for intraperitoneal injection. Blood glucose levels at 15, 30, 60, and 120 mins were measured and recorded, ITT curves were drawn, and AUC was calculated. Homeostasis Model Assessment-Insulin Resistance value (HOMA-IR) was determined as the following formula:

$$\mathrm{HOMA-IR} = \frac{\textit{fasting blood glucose } (mmol/L) * \textit{ fasting insulin concentration } (mU/L)}{22.5}$$

2.4. Cell culture and cell and treatment

Human intestinal epithelial cell (HIEC) was obtained from the American Type Culture Collection (ATCC, Manassas, VA, USA). The cells were cultured in the Roswell Park Memorial Institute 1640 (RPMI 1640) media supplemented with 10% fetal bovine serum (FBS, PAN, Germany) and 1% penicillin and streptomycin under a 5% CO_2 and 37°C atmospheres. The cells were treated with palmitic acid (PA, 50 μM) before harvest to perform the H2K27ac chip experiments.

2.5. 16s rRNA

The bacterial genomic DNA of the sample was extracted using the CTAB or SDS method, and then the purity and concentration of the DNA were assessed using agar gel electrophoresis. The appropriate amounts of samples were diluted to 1 ng/μl with sterile water. Diluted genomic DNA was a template for PCR amplification using Phusion High-Fidelity PCR Master with GC Buffer from New England Biolabs. Specific primers with Barcodes were used based on the selection of sequencing areas: 16S V4 region primer was 515F-806R, 16S V3-V4 region primer was 338F-806R, 18S V4 region primer was 528F-706R, 18S V9 zone primer was 1380F-1510R, ITS1 zone primer was ITS1F-ITS2, and ITS2 zone primer was ITS2-3F-ITS2-4R. PCR products used a 2% concentration of agar gel for electrophoresis testing. A library was built using New England Biolabs' NEB Next Ultra DNA Library Prep Kit for Illumina library kits. This was quantified and library-tested by Qubit, and then MiSeq was used for onboard sequencing. The raw sequencing data was then cleaned. The OTUs (Operational Taxonomic Units) and species classification analyses were then performed based on the cleaned data, combining OTUs and species annotations to obtain the basic analysis results of OTUs and classification lineages for each sample. Then, OTUs were analyzed for abundance, diversity index, etc., and a statistical analysis of the microbial community structure was carried out on species annotations at various classification levels.

2.6. Western blot

RIPA lysis buffer (1M Tris Hcl pH 7.4, 5M Nacl, 10% Na-Deoxycholale, 10% SDS, 10% Triton X-100, and 0.5M EDTA) containing protease and phosphatase inhibitors (Bimake) was used to extracted protein from tissue. Then, a BCA assay kit (Beyotime Biotechnology, China) was used to detect the concentration of the centrifuged protein. Quantified protein was loaded onto SDS-PAGE and transferred to a PVDF membrane. After 1 h block using 5% skimmed milk, each corresponding primary antibody was added, including anti-HDAC3 (1:1000, Catalog#:12829, Cell Signaling Technology), anti-CD36 (1:1000, Catalog#: ab154786, Abcam), anti-IRS1(1:1000, Catalog#:2382, Cell Signaling Technology), anti-p-IRS1(1:1000, Catalog#:2384, Cell Signaling Technology), anti-PI3K(1:1000, Catalog#:4292, Cell Signaling Technology), anti-p-PI3K(1:1000, Catalog#:17366, Cell Signaling Technology), anti-AKT(1:1000, Catalog#:4691, Cell Signaling Technology), anti-p -AKT(1:1000, Catalog#:4060, Cell Signaling Technology), and β-actin (1:1000, Catalog#: GB11001, Servicebio), and incubated at 4°C overnight. The next day, band density was calculated by ChemiDoc XRS+ (Bio-Rad, USA) following 1 h secondary antibody incubation.

2.7. qRT-PCR

TRIzol reagent (Invitrogen, USA) was used to extract the RNA of mice tissue and cultured cells according to the manufacturer's instructions. Subsequently, the RNA was reversely transcribed to cDNA using SYBR® Green Premix Pro Taq HS qPCR Kit (Cat No. AG11701, AG) and amplified by a C1000 Thermal Cycler (Bio-Rad). GAPDH was used as an internal reference, and its primer pairs were as follows: forward: 5' TGTGTCCGTCGTGGATCTGA 3', reverse: 5' TTGCTGTTGAAGTCGCAGGAG 3'. The primer pairs of the target genes were as follows: HDAC3: forward: 5' GCACCCAGTGTCCAGATTCA 3', reverse: 5' GACCTCTCTCTTCAGCGTCG 3'; CD36: forward: 5' GGTCTATCTACGCTGTGTTCGG 3', reverse: 5' TCTGGATTCTGGAGGGGTGA 3'.

2.8. ChIP-qPCR

Chip-qPCR was performed as described in our previous study [29]. The anti-H3K27ac (Catalog#:8173, Cell Signaling Technology, 1 μg/test) and control IgG (Catalog#:3900, Cell Signaling Technology, 1 μg/test) were used for the ChIP experiment. Then, qRT-PCR was performed to quantify the relative enrichment at the enhancer region of the precipitated target gene. Percentages of input DNA were used to calculate and quantify relative abundance. Its primer pairs were as follows: PPAR-γ: forward: 5' ACCAAAGTGCAATCAAAGTGGA 3', reverse: 5' ATGAGGGAGTTGGAAGGCTCT 3'.

2.9. Immunohistochemistry

Fresh intestinal tissue was collected, cut into 2 cm segments, and soaked with paraformaldehyde. Samples were paraffin-embedded and sectioned into 4 μm-thick slices. The tissue sections were 'deparaffinized' and rehydrated, placed in a repair box filled with citric acid (pH6.0) antigen retrieval buffer for antigen retrieval in a microwave oven, and then placed in 3% hydrogen peroxide to block endogenous peroxidase activity. After serum sealing, the sections were incubated overnight at 4°C with primary antibody including anti-HDAC3 (1:200, Catalog#: ab32369, Abcam), anti-CD36 (1:200, Catalog#:28109, Cell Signaling Technology). The next day, sections were washed with PBS (pH7.4), and incubated with a secondary antibody at room temperature for 60 minutes. Then, DAB staining and hematoxylin staining were applied to the sections before dehydration and mounting. The results were displayed by an imaging system (Nikon DS-U3, Japan Nikon).

2.10. Metabolomic analysis

For tissue and fecal sample preparation, 30 mg of weighted samples were transferred into a 2 ml Eppendorf tube containing 200 μL sodium hydroxide (1M), 200 μL methanol, and 20 μL internal standard (D4-alanine, 10 mM). Samples were then homogenized using Tissuelyser II (QIAGEN, USA) and the supernatant was isolated by centrifugation at 15000 rpm, 4°C for 20 min. The supernatants were carefully transferred into new tubes and dehydrated by SpeedVac (Labconco, USA) prior to chemical derivatization. As described in previous publications, lyophilized samples were derivatized through the methyl chloroformate (MCF) method (11) [30]. Next, chemical derivatives were analyzed by a system of Agilent GC-MS instrument (GC7890B-5977A) using a ZB-1701 GC capillary column (30 m × 250 μm id × 0.15 μm with 5-m guard column, Phenomenex, CA, USA). The mass selective detector (EI) was at 70 eV, and other GC-MS parameters were applied according to a previously published article (11). The MassOmics XCMS R-based software was used to calculate the abundance of each metabolite through the areas under each identified peak. The relatively identified compounds were normalized by an internal standard (2,3,3,3-d4-alanine), and biomass (mg) was applied to correct the differential size effect of the tissues and feces.

Prior to data analysis, each identified metabolite was transformed by the $\log_{10}$ scale and Pareto scaled to ensure a normal distribution of the dataset. The metabolite profiles of tissue and

faece were compared by Principal component analysis (PCA) in R. Student's t-tests (*P*-values less than 0.05) were applied to evaluate the significant difference between the normal group and the GDM group. The correction of multiple comparisons was done by using false discovery rates (FDR, q-value) R-packages. The heatmap between the two groups was obtained from the ggplot2 R-package. pROC R-package was used to calculate the receiver operating characteristic (ROC) curves. Pathway enrichment analysis was performed by the Kyoto Encyclopedia of Genes and Genomes (KEGG) database, and the corrplot R package was used for Pearson's correlation analysis.

2.11. ELISA enzyme-linked immunosorbent assay (ELISA)

In the mouse models, the ELISA assay was performed to examine the concentration of SCFA, ApoB48, triglyceride, free fatty acid, and insulin in serum (Jianglai Biotechnology, China). The serum samples were removed from a −80°Crefrigerator and melted in the ice. The procedures were performed following the manufacturer's instructions for the kit. Finally, the OD value was detected at 450 nm wavelength. The serum concentrations of SCFA, ApoB48, and insulin were calculated according to the standard curves, respectively. ELISA kits (Solarbio, China) were used and performed according to the manufacturer's protocols for the level of TG and TC detection in peripheral tissues.

3. Results

3.1. The high-fat diet was used to construct the GDM mice model

As shown in Figure 1A, a high-fat diet-induced GDM mouse model was utilized in our experiment. The weight of the GDM and NC groups was monitored during pregnancy. The results showed that the weight at D 18.5 and pregnancy weight gain of the GDM group were significantly higher than those of the NC group, while there was no significant difference between the two groups at D0.5 (Fig. 1C). OGTT and ITT were performed at D0.5, D11.5 and D16.5, respectively, and the area under the curve (AUC) of blood glucose value was calculated. OGTT results showed that the fasting blood glucose and the blood glucose values at D11.5 and D16.5 of the GDM group were significantly higher than those in the NC group (Fig. 1D). There was no statistical significance in the OGTT value and AUC at D0.5 in both groups (Fig. 1D). Moreover, there was no significant difference in ITT value and AUC between GDM and NC groups at D0.5 (Fig. 1E). These results suggested low insulin sensitivity in GDM mice after D11.5. Moreover, we recorded fast blood glucose and serum insulin concentration through ELISA. Then we compared insulin sensitivity using the homeostasis model assessment insulin resistance (HOMA-IR). We found fast blood glucose and serum insulin concentrations were higher in the HFD group than in the NC group (Fig. 1B). Additionally, the HOMA-IR value in the HFD group increased significantly, meaning the GDM group apparently suffered from insulin resistance. Therefore, we have successfully established mice fed with an HFD as the GDM group.

3.2. The intestinal flora of GDM mice significantly differed from that of the NC group

To evaluate the differences in gut microbes between GDM and NC groups, we performed a 16s rRNA sequence. We found that the bacteria in the GDM group and the NC group mainly identified as *Actinobacteria, Bacteroidetes, Deferribacteres, Firmicutes, Proteobacteria, Spirochaetes* and other categories, among which *Firmicutes* and *Bacteroidetes* had obvious differences in proportion (Fig. 2A, B). The ratio of *Firmicutes* to *Bacteroidetes* in the GDM group was significantly higher than in the NC group (Fig. 2C). LEfSe analysis showed that the level of *Firmicutes* in the GDM group was significantly higher than that in the NC group on the category level (Fig. 2D). On the genus level, the abundance of *Butyricimonas* in the GDM group was significantly lower than that in the NC group, while *Lactococcus, Roseburia, Ruminococcus, Oscillospira*, and *SMB53* were on the contrary (Fig. 2D). Furthermore, solid-phase microextraction was used for the quantitative detection of SCFA in the feces of the two groups by GC-MS analysis (Fig. 2E). The results showed that the concentrations of propionic acid and butyric acid were lower in the GDM group compared with the NC group (Fig. 2E). Noticeably, the correlation analysis (Fig. 2F) also suggested *Firmicutes* have a significant positive correlation with stearic acid. In addition, the genus *Butyricoccus* was positively correlated with both propionic and butyric acids, highly correlated with butyric acids, and moderately correlated with propionic acids, and levels of *Butyricoccus* were higher in the NC group (Fig. 2F). These findings observed dysbiosis of the gut microbiota and SCFA concentrations among GDM mice.

3.3. Metabolite profiles of intestinal tissue and stool

We performed GC-MS-based metabolomics to explore whether changing intestinal flora would disturb the metabolite composition of intestinal tissue and stool between normal and GDM groups. A total of 208 compounds in the gut tissue and 198 metabolites in the stool were identified, respectively. Principal component analysis (PCA) was used to diversify the characteristics of stool and tissue metabolic profiles, and the result showed that the SI_NC group, SI_GDM, Co_NC group and Co_GDM group were clustered separately (Figure 3A; SI: Small intestine; Co: Colon). The heatmap showed that there was a number of significantly different metabolites between GDM and NC groups in the gut as well as their corresponding faeces, including three benzoic acids and derivatives, two amino acids and derivatives, seven saturated fatty acids, one keto acid and derivatives, one tricarboxylic acid and derivatives, fifteen unsaturated long−chain fatty acids, three SCFA derivatives, two nicotinamides and Vitamines, one carboxylic acid, and derivatives, one medium−chain fatty acids, fourteen organic compounds (Fig. 3B). Interestingly, there were twenty-one metabolites with an area under the receiver operating characteristic (ROC) curve greater than 0.95 in the gut. Fourteen and seven metabolites were shortlisted in the small and large intestines, respectively. These included six unsaturated fatty acids, five organic compounds, two SCFAs, five LCFAs, two saturated fatty acids and one nicotinamide and vitamin. What is more, there were twenty-two metabolites with an area under the ROC curve greater than 0.9 in feces. These included six saturated fatty acids, three medium chain fatty acids, two benzoic acids and their derivatives, one TCA derivative, and one nicotinamide and vitamin. According to KEGG pathway analysis, we found lipid metabolism pathways were upregulated in small intestine tissue and faeces, including biosynthesis of unsaturated fatty acids, metabolism of linoleic acid, and metabolism of arachidonic acid, and these associated metabolites were all increased in the GDM group (Fig. 3D). These data indicated that the concentrations of SCFAs were reduced, whereas LCFAs (e.g., palmitic acid and stearic acid, Fig. 3C) were increased in the GDM group compared to the NC group.

3.4. Elevation of HDAC3 and CD36 promoted absorption and transport of fatty acids in the GDM group

From qRT-PCR and western blotting results, we found that the relative expression of HDAC3 and CD36 in the GDM group was

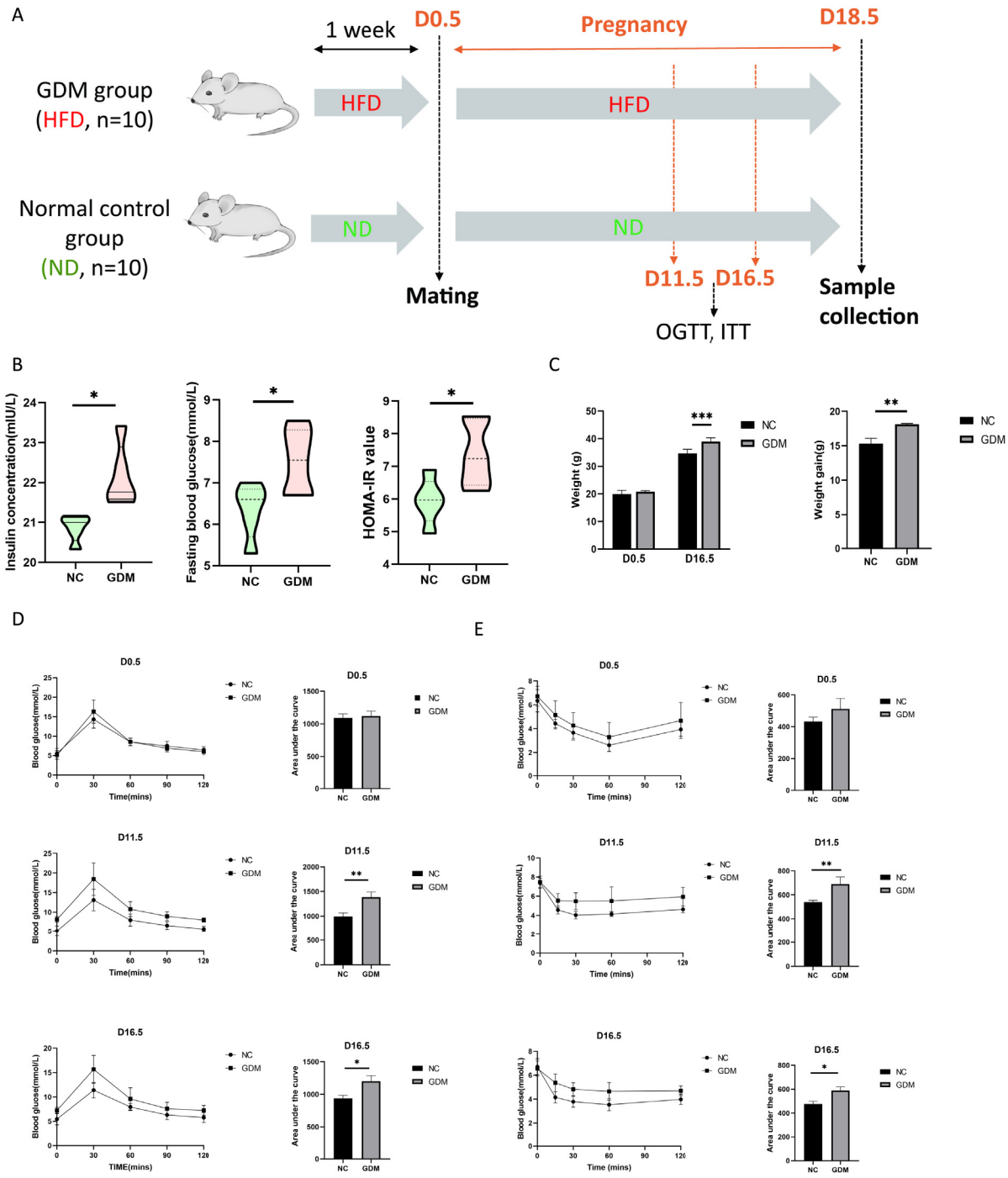

Fig. 1. GDM mice model construct and evaluate. (A) Schematic representation of GDM mice model and experiment. (B) Fasting plasma glucose, serum insulin, and HOMA-IR value were measured by ELISA. (C) The change of weight of the HFD and NC groups during pregnancy. (D, E) OGTT and ITT were detected at D0.5, D11.5 and D16.5 respectively. Results are shown as mean ± SEM, n=6, $^{*}P<.05$, $^{**}P<.01$ and $^{***}P<.001$.

higher than that in the NC group at both mRNA and protein levels, while the expressions of H3K27ac and PPAR-γ were on the contrary (Fig. 4C, D, F). Immunohistochemical staining also showed that HDAC3 and CD36 were distributed in the epithelial cells of the small intestine and colon, and the expression in the GDM group was significantly higher than that in the normal group (Fig. 4A, B). The result of H3K27ac ChIP-qPCR showed that palmitic acid treatment reduced the enrichment at the enhancer region of PPAR-γ in human intestinal epithelial cells (Fig. 4E). To explore the effect of a high-fat diet on intestinal fatty acid absorption, we used ELISA kits to measure the serum concentrations of free fatty acid (FFA), triglyceride (TG), ApoB48, and short-chain fatty acid (SCFA). The result showed that FFA, TG, and ApoB48 concentration was higher in the GDM group, while the concentration of SCFA in the serum of the GDM group was lower than that in the NC group (Fig. 4G). Thus, it was indicated that the GDM group could transport more fatty acids into the blood circulation, and this phenomenon may be due to the activation of CD36.

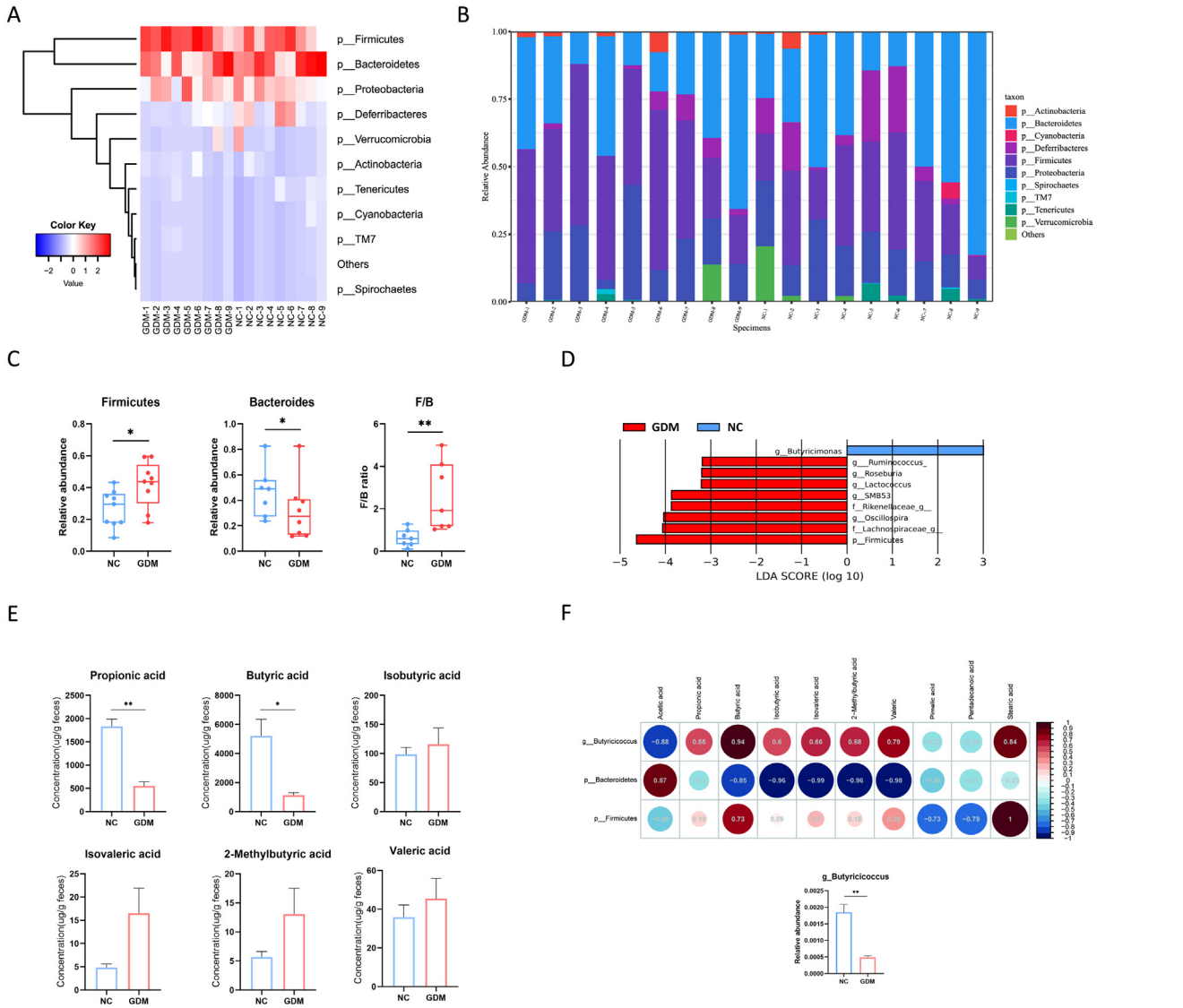

Fig. 2. The characteristics of the 16s rRNA sequencing data. (A) Heatmap of relative abundance of gut microbiota in fecal samples at phylum level. (B) Taxonomy plot of relative abundance of gut microbiota in fecal samples at phylum level. (C) Relative abundance of *Firmicutes* and *Bacteroidetes* and the ratio of *Firmicutes*/*Bacteroidetes*(F/B). (D) The bacterial taxa whose levels differed significantly between the NC and GDM groups were identified by linear discriminant analysis (LDA) using LEfSe. (E) Levels of propionic, butyric, isobutyric, isovaleric, 2-methylbutyric, and valeric acids in mice feces. (F) Heatmap of correlations between bacterial genera/phyla and SCFAs in feces. The color indicates the correlation coefficients (blue, negative; red, positive).

3.5. HFD impaired the insulin response pathway

We detect the levels of TG and TC in the liver and muscle. According to our ELISA results, the abundance of TG and TC was significantly elevated in the liver of the GDM group versus the NC group (Supplementary Fig. S1). To evaluate insulin sensitivity and glucose transport of the insulin-targeted organs, including adipose, liver, and muscle tissues in GDM group mice, we examined the PI3K/AKT pathway protein expression (IRS-1, p-IRS-1, PI3K, p-PI3K, AKT, p-AKT) by western blot in Figure 5. We found that p-IRS-1, p-PI3K, and p-AKT had significantly reduced expression in the GDM group compared with the NC group. These results indicated that the insulin signaling pathway and glucose transportation were dysregulated in the GDM mice group.

3.6. GDM-FMT mice developed insulin resistance

To further explore whether gut microbiota regulates the GDM process, mice were treated with antibiotics for 5 days, followed by FMT, which was derived from normoglycemic pregnant women or GDM pregnant women, and divided these mice into 3 groups (GDM-FMT, Normal-FMT, and Control-FMT groups). OGTT and ITT were performed at GD 0.5, 11.5 and 16.5 to evaluate blood glucose and insulin sensitivity, and the GDM-FMT group showed lower glucose tolerance and insulin sensitivity versus Normal-FMT and Control-FMT groups (Figure S2A, S2B). To evaluate the differences in gut microbes between FMT groups, we performed a 16s rRNA sequence. The ratio of *Firmicutes* to *Bacteroidetes* in the GDM-FMT group was significantly higher than in Control-FMT and Normal-

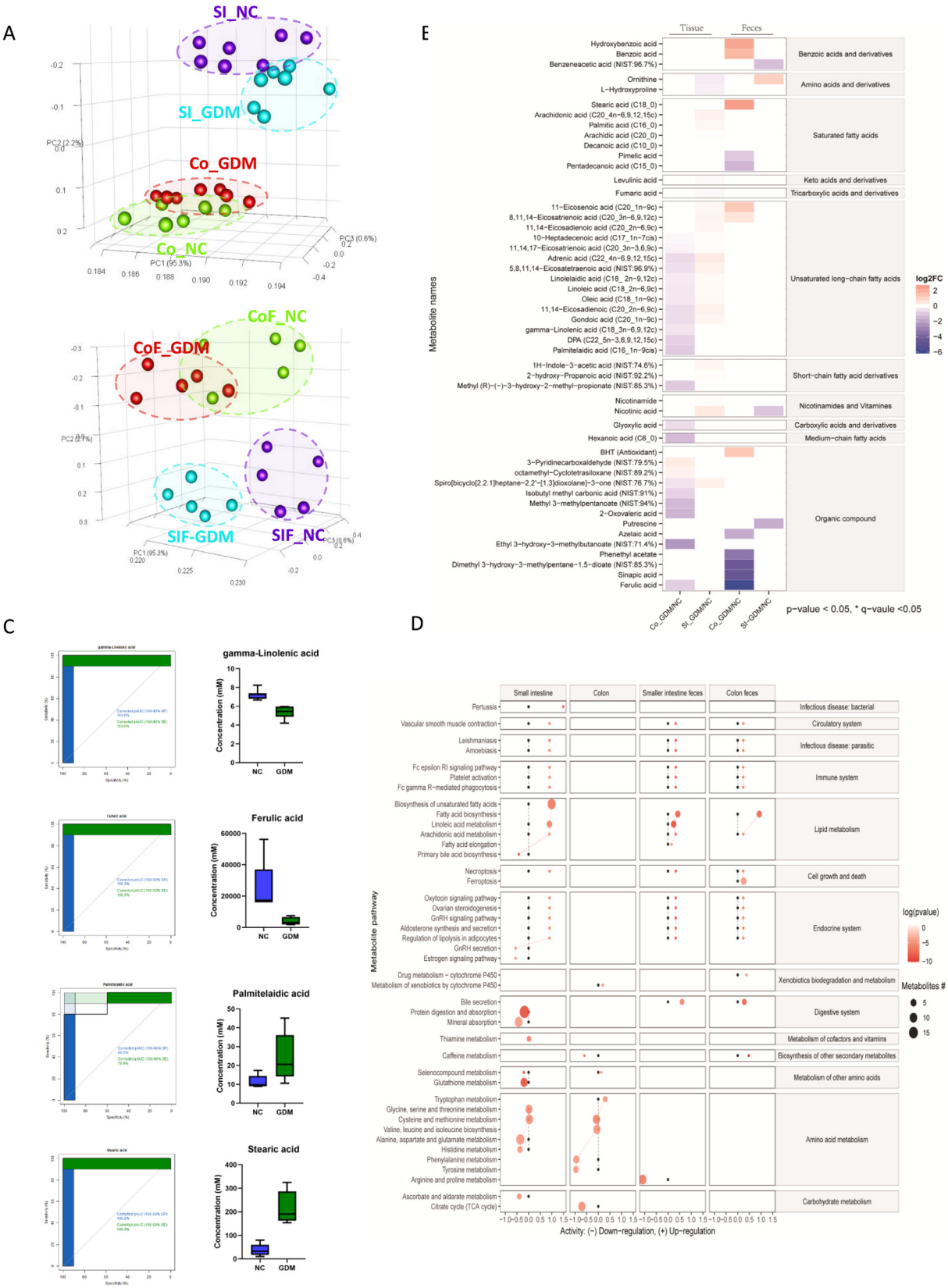

Fig. 3. The characteristics of the intestinal tissue and feces metabolic data. (A) The principal component analysis (PCA) of all metabolites in intestinal tissue and feces. (B) The heatmap of the significantly changed metabolites in intestinal tissue and feces. The red blocks represent higher metabolite concentrations in the GDM group than in the NC group, and the blue blocks represent lower metabolite concentrations in the GDM group than in the NC group. (C) Area under the receiver operating characteristic (ROC) curve for intestinal tissue and feces metabolites. There were 4 metabolites with an area under the ROC curve greater than 0.95. (D) Pathway analysis of significantly altered metabolites by R package ($P<.05$ by the Student's t-test). The red circle represents the GDM group, and the black circle represents the NC group.

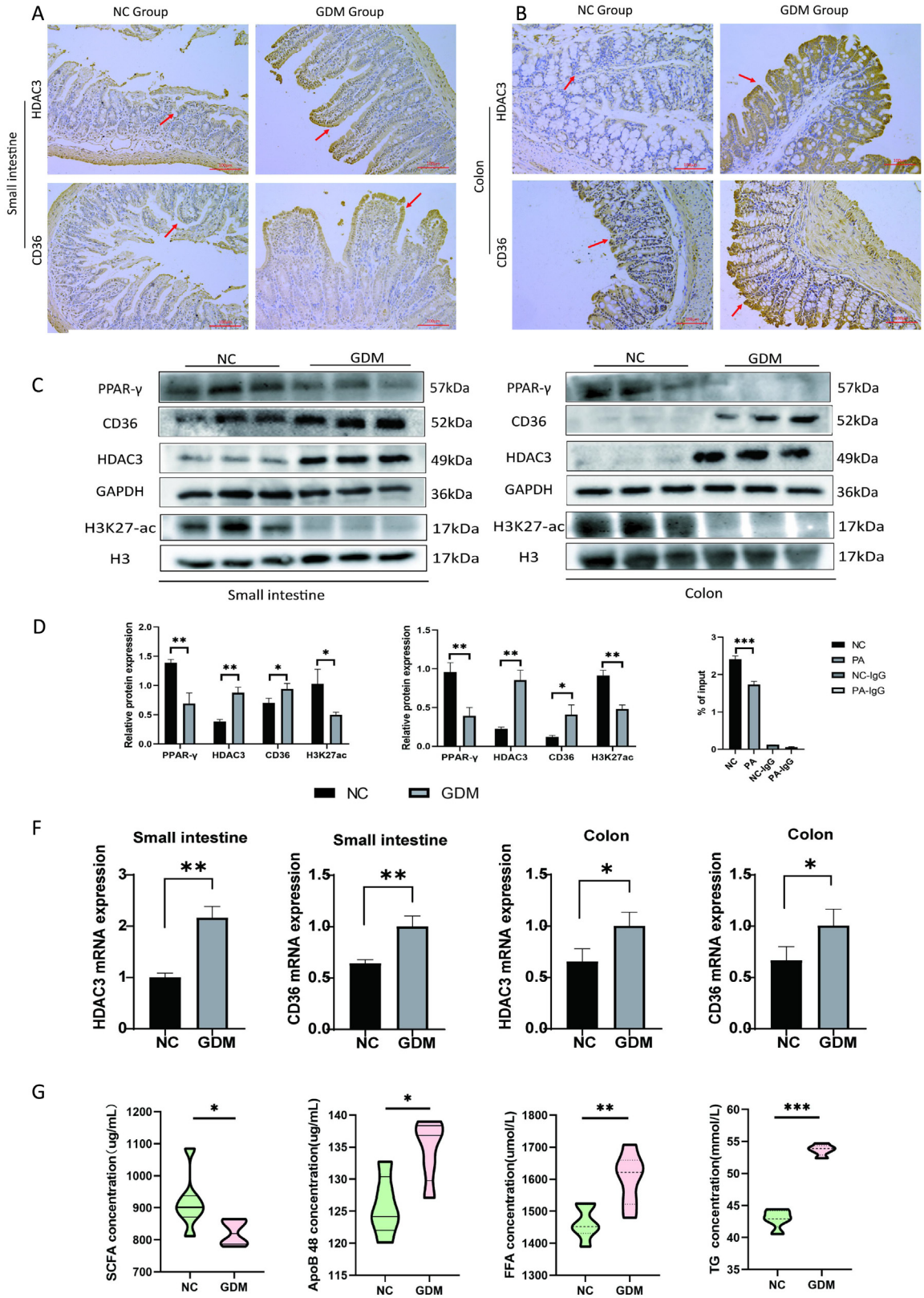

Fig. 4. HFD results in excessive lipid transportation from the intestinal into blood circulation. (A, B) Immunohistochemistry analysis of CD36 and HDAC3 in the intestinal. (C-D) Western blot analysis of CD36, HDAC3, H3K27ac, and PPAR-γ. (C) qPCR for detecting mRNA levels of the CD36 and HDAC3 in the intestine. (E) ChIP-qPCR for H3K27ac represented H3K27ac enrichment on PPAR-γ enhancers. (F) qPCR for detecting mRNA levels of the CD36 and HDAC3 in the intestine. (G) ELISA analysis for the SCFA, ApoB 48, FFA, and TG levels in the serum. Results are shown as mean ± SEM, $^{*}P<.05$, $^{**}P<.01$ and $^{***}P<.001$.

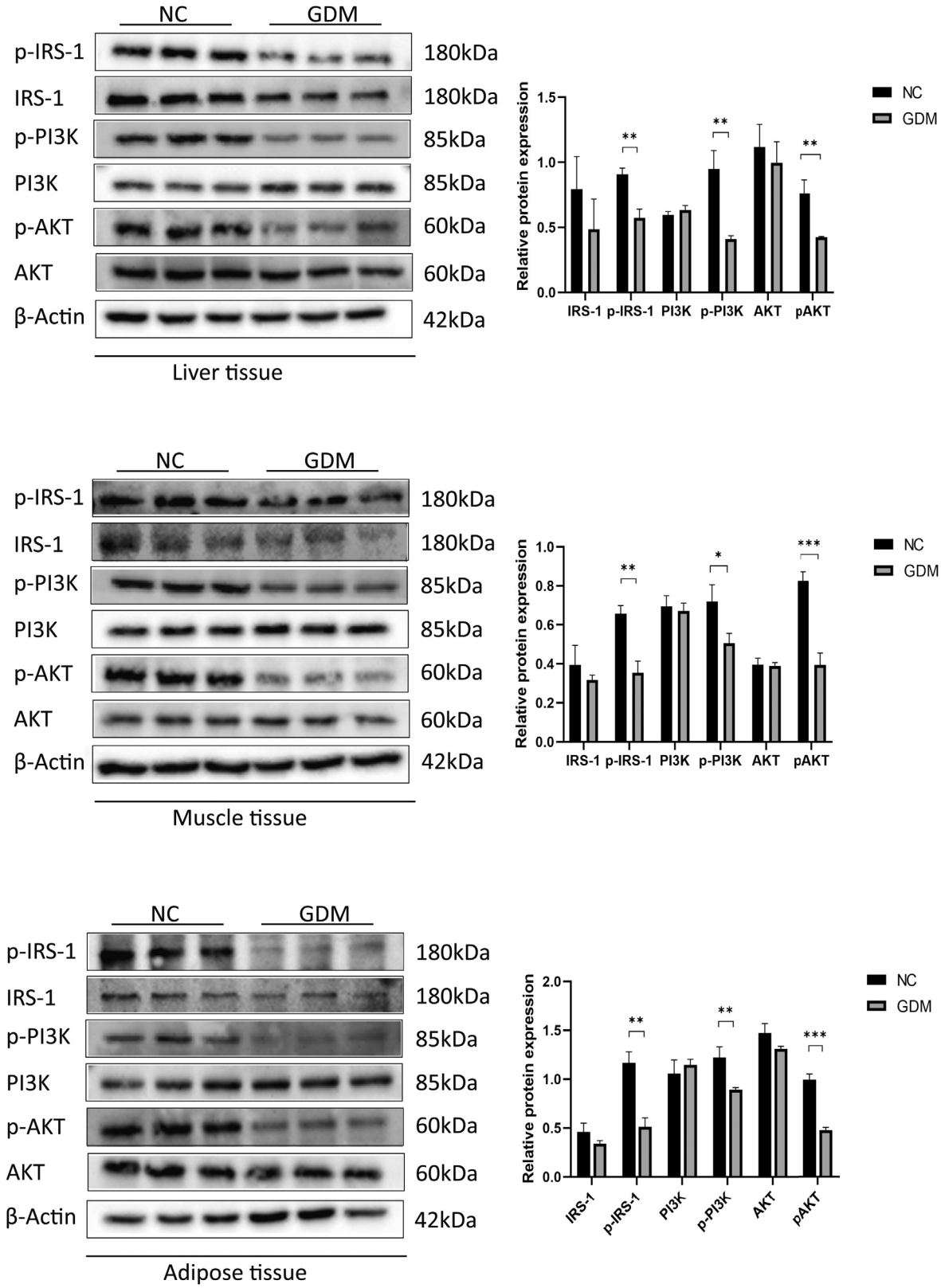

Fig. 5. Deregulate insulin pathway in the liver, muscle, and adipose tissue in the GDM group. (A-C) Western blot analysis showed the IRS/p-IRS, PI3K/p-PI3K, and AKT/p-AKT levels in liver (A), muscle (B) and adipose (C) tissue. Results are shown as mean ± SEM, n=3, $^{*}P<.05$, $^{**}P<.01$ and $^{***}P<.001$.

FMT groups (Supplementary Fig. S3A). We found a clear difference in the proportion of *Firmicutes* and *Bacteroidetes* between GDM-FMT, Control-FMT and Normal-FMT groups (Supplementary Fig. S3B). LEfSe analysis showed that the level of *Bacteroidetes* in the Control-FMT group was significantly higher than that in the other two groups on the phylum level (Supplementary Fig. S3C). Next, we performed GC-MS to detect the abundance of SCFAs, and we found the levels of propionic acid and butyric acid were lower in the GDM-FMT group versus the Control-FMT and Normal-FMT groups (Fig. 6A). From our western blot results in the intestinal tissues, we found that the expression of HDAC3 and CD36 in the GDM-FMT group was higher than that in the Control-FMT and Normal-FMT groups, while the expressions of H3K27ac and PPAR-γ were on the contrary (Fig. 6B, C). Then, we detect the levels of TG and TC in mice liver and muscle after FMT. According to our ELISA results, the abundance of TG and TC was significantly increased in the liver of the GDM-FMT group versus the Normal-FMT and Control-FMT groups (Fig. 6D). Further analysis of the expression of AKT, p-AKT, PI3K, and p-PI3K showed a notable decline of p-AKT and p-PI3K protein expression in the GDM-FMT group (Fig. 6F). To further explore the potential role of propionic acid and butyric acid on fatty acids transport, we used human intestinal epithelial cells to explore the role of propionic acid and butyric acid on the HDAC3-H3K27ac-PPAR-γ axis, and we fund the expression of HDAC3 and CD36 were inhibited after propionic acid and butyric acid treatment, while the expression of H3K27ac and PPAR-γ were on the contrary (Fig. 6G and H). These results indicated that GDM patient-derived FMT results in SCFAs decrease, lipid transport promotion, and insulin resistance in pregnant mice.

4. Discussion

In this study, we combined multi-omics to explore the potential relationship between intestinal flora and GDM metabolism. The high-fat diet-induced GDM mice model was used to investigate whether intestinal dysbiosis could contribute to abnormal circulating lipids, leading to insulin resistance and GDM. We found that a high-fat diet caused an imbalance of the intestinal flora, downregulated microbial SCFA biosynthesis, elevated free fatty acids in the blood circulation, and reduced insulin sensitivity of liver, fat, and muscle tissues. Thus, high-fat diet induced dysbiosis of the gut microbiome may contribute to the development of GDM.

Living environment factors, including dietary changes, reduced physical activity, and obesity, play a vital role in the occurrence and development of GDM [31,32]. The gut microbiota influences host metabolic and physiological functions, such as lipid, glucose, and insulin signaling, which are highly correlated with the etiology of GDM [33,34]. Differences in gut microbiome between GDM and normal pregnancy women have also been reported [18]. Our 16s rRNA sequencing results showed significant differences in the gut microbiota between the GDM and the NC groups (Fig. 2). Our results indicated that the abundance of *Firmicutes* phylum was increased, while *Bacteroides* was reduced in the GDM group compared to the control mice (Fig. 2C). At the genus level, the *Butyricmonas* decreased significantly in the GDM group. These results were consistent with previous studies that found that the ratio of Firmicutes/Bacteroides in the GDM group was elevated [35]. Additionally, much research showed that *Firmicutes phylum* promoted lipid absorption [35–37]. Other studies have demonstrated that the gut microbiome restricts lipid accumulation associated with the onset of GDM by utilizing dietary substrates to produce metabolites, such as (SCFAs), endogenously [38,39]. Thus, an abnormal proportion of gut microbiota may lead to dysregulated lipid metabolism in the development of GDM.

SCFA is a primary determinant of the production of gut microbiota involved in regulating lipid metabolism [40]. Our GC-MS results showed that propionic acid and butyric acid concentrations were significantly higher in the feces of the NC group than those in the GDM group, particularly propionic acid (Fig. 2E). The fermentation substrate of propionic acid is primarily glucose [41], which can reduce plasma fatty acid levels and inhibit liver fatty acid production by inhibiting hepatic lipolysis [42,43]. Our intestinal metabolomics pathways analysis found lipid metabolism was upregulated in the GDM group, with increased activities of biosynthesis of fatty acids and linoleic acid metabolism (Fig. 3D). In addition, we found that the anti-inflammatory unsaturated fatty acids, such as ferulic acid and linolenic acid, decreased in the GDM group, while pro-inflammation long-chain saturated fatty acids increased, such as stearic acid and palmitic acid (Fig. 3C). Furthermore, it has been reported that the gut microbiota and its metabolite SCFA synergistically regulate fatty acid metabolic processes through different signaling pathways [44]. Previous studies have shown that SCFAs can act as histone deacetylase 3 (HDAC3) inhibitors in the intestine, leading to the deacetylation of H3K27 [16]. Additionally, there is evidence that reduced H3K27ac levels hinder the expression of PPAR-γ, thus promoting the upregulation of CD36 expression [20,21,25]. These previous findings align with our results, as we observed elevated levels of HDAC3 in the GDM group, which led to reduced acetylation of H3K27 (Fig. 4C, D). Consequently, the expression of PPAR-γ was inhibited, while the level of CD36 was elevated (Fig. 4C). Due to its role as a fatty acid transporter, increased expression of CD36 has been reported to exacerbate the absorption and transport of fatty acids in the intestine [16]. Fatty acids undergo the conversion of TGs before being packaged with apolipoprotein (Apo) B48 to form chylomicrons (CM), which are finally transported into the bloodstream [45,46]. These TGs are hydrolyzed into free fatty acids (FFA) within capillaries. The resulting FFAs are then transported to the liver, muscle, and adipose tissue for storage or utilization [47,48]. Notably, our results also revealed higher ApoB48, TG, and FFA concentrations in the GDM group compared to the NC group (Fig. 4E). Therefore, the activation of HDAC3 resulting from low SCFA concentrations could contribute to increased absorption of dietary fatty acids and TGs in the gut and subsequently transport them into the blood circulation.

Elevated concentrations of fatty acids and TGs in the bloodstream lead to insulin resistance in insulin-sensitive organs. Insulin binds to the insulin receptor (IR) on the cell surface, triggering IR tyrosine/serine phosphorylation and subsequently binding to IRS-1. This binding event results in IRS-1 phosphorylation at multiple sites [49]. Consequently, PI3K and AKT, downstream of IRS-1, undergo further activation, promoting GLUT-4 translocation to regulate glucose homeostasis [50]. Our results showed increased levels of TG and TC in the peripheral tissues (Supplementary Fig. S1A), which were accompanied by reduced expression of p-IRS-1, p-PI3K and p-AKT in the liver, muscle, and adipose tissue of the GDM group (Fig. 5A-C). These results are consistent with existing literature indicating that the elevated levels of fatty acids and TGs in the circulation impaired the PI3K/AKT signaling pathway and GLUT-4 transposition, consequently limiting glucose absorption and transport [51,52]. Thus, the elevations of fatty acids and TGs in blood circulation contribute to the imbalance of glucose homeostasis and insulin resistance in insulin-target organs.

FMT derived from GDM patients causes mouse insulin resistance development. Our experiments with the FMT mouse model showed that SCFAs-producing bacteria such as *Butyricicoccaceae, Blautia,* and *Lachnospirales* reduced significantly in the GDM-FMT

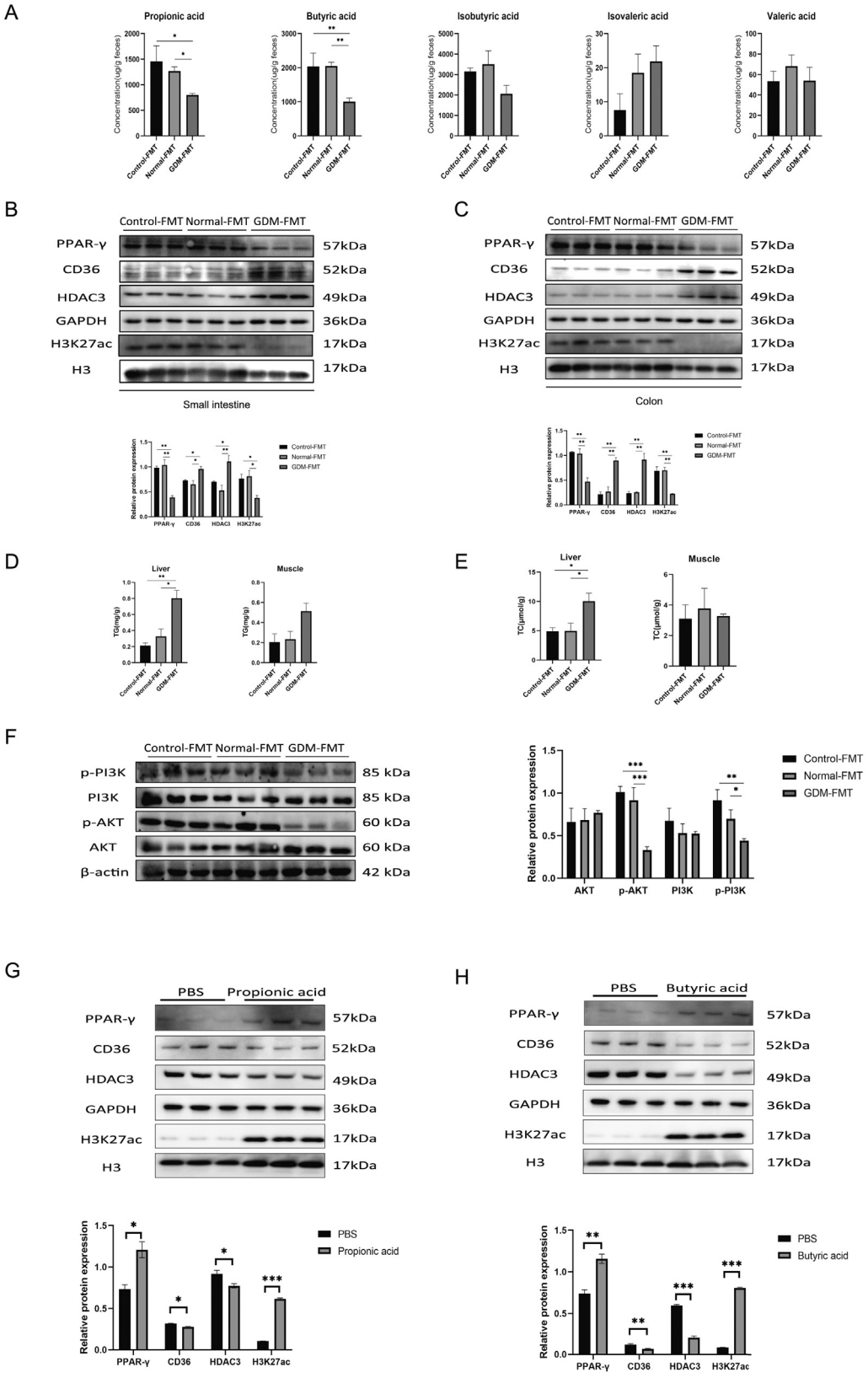

Fig. 6. GDM-FMT causes a reduction in SCFA, resulting in excessive lipid transport and impairment of insulin-responsive pathways. (A) Levels of propionic, butyric, isobutyric, isovaleric, and valeric acids in FMT mice feces. (B-C) Western blot analysis of PPAR-γ, CD36, HDAC3, and H3K27ac in the intestinal. (D-E) ELISA analysis for the level of TG (D), and TC (E) in the liver and muscle. (F) Western blot analysis showed the PI3K/*p*-PI3K and AKT/*p*-AKT levels in the liver. (G-H) Western blot analysis of PPAR-γ, CD36, HDAC3, and H3K27ac in human intestinal epithelial cells after treatment of propionic (G) and butyric (H) acids. Results are shown as mean ± SEM, $^{*}P<.05$, $^{**}P<.01$ and $^{***}P<.001$.

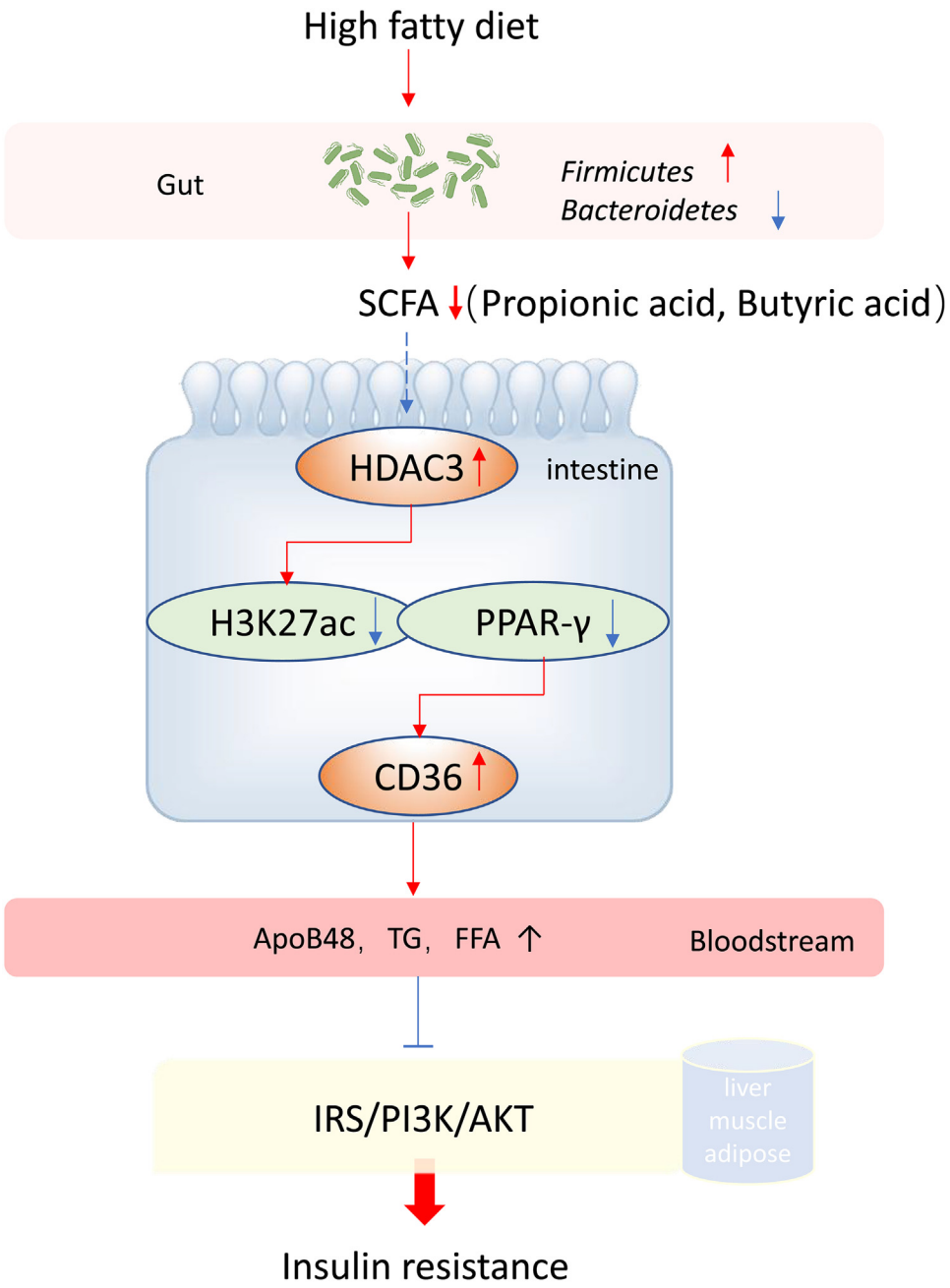

Fig. 7. HFD-induced decreased gut microbiota-derived short-chain fatty acids elevate lipid transportation into blood circulation.

group. These phenomena were satisfied with the fecal microbiota composition of our GDM mouse model and consistent with previous studies that SCFAs-producing bacteria decreased in GDM patients [34]. Interestingly, we also found that HDAC3 and CD36 protein levels in the gut tissues of the GDM-FMT group were significantly increased, while the protein levels of H3K27ac and PPAR-γ were remarkably decreased. Notably, the abundance of TG and TC in the liver of the GDM-FMT group was accompanied by impaired insulin sensitivity, and these findings were similar to the GDM mouse model. Moreover, SCFA treatment inhibited lipid transport-related protein expression. These results indicated that GDM patient-derived FMT promoted GDM development, which may be partially attributed to the increased lipid transport caused by reduced SCFA.

In conclusion, as shown in Figure 7, a high-fat diet disrupts the compositions of intestinal flora and reduces SCFA levels, leading to the activation of HDAC3. This, in turn, inhibits the acetylation of H3K27. Decreased H3K27ac levels downregulate the expression of PPAR-γ and further upregulate CD36 to facilitate the absorption and transport of lipids into the blood circulation. Thereafter, the elevated levels of FFAs and TGs in the bloodstream impede insulin sensitivity in the target organs. Understanding the associations between the gut-insulin targeted organ axis will contribute to our comprehension of the pathophysiology process involved in GDM.

Declaration of generative AI

This manuscript is not created by AI.

Declarations of competing interest

There are no competing interests.

CRediT authorship contribution statement

Hao Chen: Writing – review & editing, Writing – original draft, Methodology, Investigation, Formal analysis, Data curation, Conceptualization. **Shi-Han Wang:** Writing – original draft, Methodology, Formal analysis, Data curation, Conceptualization. **Hong-Li Li:** Writing – original draft, Methodology, Formal analysis, Data curation, Conceptualization. **Xiao-Bo Zhou:** Supervision. **Lin-Wei Zhou:** Methodology, Formal analysis, Data curation, Conceptualization. **Chang Chen:** Supervision. **Toby Mansell:** Supervision. **Boris Novakovic:** Supervision. **Richard Saffery:** Supervision. **Philip N. Baker:** Supervision. **Ting-Li Han:** Writing – review & editing, Writing – original draft, Supervision. **Hua Zhang:** Supervision, Project administration, Funding acquisition, Conceptualization.

Acknowledgments

This work was supported by the National Natural Science Foundation of China (No. 81971406, 81771607, 81871185, 81901507, 81961128004), The 111 Project (Yuwaizhuan (2016)32), Chongqing Health Commission (2018ZDXM024), Chongqing Health Commission and Chongqing Science & Technology Commission (2021MSXM121, 2020MSXM101, KJZD-K202100407), Chongqing Graduate Research Innovation Project (CYS21218).

Supplementary materials

Supplementary material associated with this article can be found, in the online version, at doi:10.1016/j.jnutbio.2024.109708.

References

[1] Huang L, Thonusin C, Chattipakorn N, Chattipakorn SC. Impacts of gut microbiota on gestational diabetes mellitus: a comprehensive review. Eur J Nutr 2021;60:2343–60. doi:10.1007/s00394-021-02483-6.
[2] Cortez RV, Taddei CR, Sparvoli LG, Ângelo AGS, Padilha M, Mattar R, et al. Microbiome and its relation to gestational diabetes. Endocrine 2019;64:254–64. doi:10.1007/s12020-018-1813-z.
[3] Di Cianni G, Miccoli R, Volpe L, Lencioni C, Del Prato S. Intermediate metabolism in normal pregnancy and in gestational diabetes. Diabetes Metab Res Rev 2003;19:259–70. doi:10.1002/dmrr.390.
[4] Zhu WW, Yang HX, Wei YM, Yan J, Wang ZL, Li XL, et al. Evaluation of the value of fasting plasma glucose in the first prenatal visit to diagnose gestational diabetes mellitus in china. Diabetes Care 2013;36:586–90. doi:10.2337/dc12-1157.
[5] Ponzo V, Fedele D, Goitre I, Leone F, Lezo A, Monzeglio C, et al. Diet-gut microbiota interactions and gestational diabetes mellitus (GDM). Nutrients 2019;11(2):330. doi:10.3390/nu11020330.
[6] Wang J, Zheng J, Shi W, Du N, Xu X, Zhang Y, et al. Dysbiosis of maternal and neonatal microbiota associated with gestational diabetes mellitus. Gut 2018;67:1614–25. doi:10.1136/gutjnl-2018-315988.
[7] Voigt RM, Forsyth CB, Green SJ, Engen PA, Keshavarzian A. Circadian rhythm and the gut microbiome. Int Rev Neurobiol 2016;131:193–205. doi:10.1016/bs.irn.2016.07.002.
[8] Nobs SP, Tuganbaev T, Elinav E. Microbiome diurnal rhythmicity and its impact on host physiology and disease risk. EMBO Rep 2019;20(4):e47129. doi:10.15252/embr.201847129.
[9] Whitman WB, Coleman DC, Wiebe WJ. Prokaryotes: the unseen majority. Proc Natl Acad Sci USA 1998;95:6578–83. doi:10.1073/pnas.95.12.6578.
[10] Mulders RJ, de Git KCG, Schéle E, Dickson SL, Sanz Y, Adan RAH. Microbiota in obesity: interactions with enteroendocrine, immune and central nervous systems. Obes Rev 2018;19:435–51. doi:10.1111/obr.12661.
[11] Simon AK, Hollander GA, McMichael A. Evolution of the immune system in humans from infancy to old age. Proc Biol Sci 2015;282:20143085. doi:10.1098/rspb.2014.3085.
[12] Kong C, Gao R, Yan X, Huang L, Qin H. Probiotics improve gut microbiota dysbiosis in obese mice fed a high-fat or high-sucrose diet. Nutrition 2019;60:175–84. doi:10.1016/j.nut.2018.10.002.
[13] Mokkala K, Houttu N, Vahlberg T, Munukka E, Rönnemaa T, Laitinen K. Gut microbiota aberrations precede diagnosis of gestational diabetes mellitus. Acta Diabetol 2017;54:1147–9. doi:10.1007/s00592-017-1056-0.
[14] Kuang YS, Lu JH, Li SH, Li JH, Yuan MY, He JR, et al. Connections between the human gut microbiome and gestational diabetes mellitus. Gigascience 2017;6:1–12. doi:10.1093/gigascience/gix058.
[15] Aberdein N, Schweizer M, Ball D. Sodium acetate decreases phosphorylation of hormone sensitive lipase in isoproterenol-stimulated 3T3-L1 mature adipocytes. Adipocyte 2014;3:121–5. doi:10.4161/adip.27936.
[16] Koh A, De Vadder F, Kovatcheva-Datchary P, Bäckhed F. From dietary fiber to host physiology: short-chain fatty acids as key bacterial metabolites. Cell 2016;165:1332–45. doi:10.1016/j.cell.2016.05.041.
[17] He J, Zhang P, Shen L, Niu L, Tan Y, Chen L, et al. Short-chain fatty acids and their association with signalling pathways in inflammation, glucose and lipid metabolism. Int J Mol Sci 2020;21(17):6134. doi:10.3390/ijms21176356.
[18] Baothman OA, Zamzami MA, Taher I, Abubaker J, Abu-Farha M. The role of Gut Microbiota in the development of obesity and diabetes. Lipids Health Dis 2016;15:108. doi:10.1186/s12944-016-0278-4.
[19] Mlodawska OW, Saini P, Parker JB, Wei JJ, Bulun SE, Simon MA, et al. Epigenomic and enhancer dysregulation in uterine leiomyomas. Hum Reprod Update 2022;28:518–47. doi:10.1093/humupd/dmac008.
[20] John E, Wienecke-Baldacchino A, Liivrand M, Heinäniemi M, Carlberg C, Sinkkonen L. Dataset integration identifies transcriptional regulation of microRNA genes by PPARγ in differentiating mouse 3T3-L1 adipocytes. Nucleic Acids Res 2012;40:4446–60. doi:10.1093/nar/gks025.
[21] Qiao Y, Kang K, Giannopoulou E, Fang C, Ivashkiv LB. IFN-γ induces histone 3 lysine 27 trimethylation in a small subset of promoters to stably silence gene expression in human macrophages. Cell Rep 2016;16:3121–9. doi:10.1016/j.celrep.2016.08.051.
[22] Oh HYP, Visvalingam V, Wahli W. The PPAR-microbiota-metabolic organ trilogy to fine-tune physiology. Faseb j 2019;33:9706–30. doi:10.1096/fj.201802681RR.
[23] Wächtershäuser A, Loitsch SM, Stein J. PPAR-gamma is selectively upregulated in Caco-2 cells by butyrate. Biochem Biophys Res Commun 2000;272:380–5. doi:10.1006/bbrc.2000.2793.
[24] Nepelska M, de Wouters T, Jacouton E, Béguet-Crespel F, Lapaque N, Doré J, et al. Commensal gut bacteria modulate phosphorylation-dependent PPARγ transcriptional activity in human intestinal epithelial cells. Sci Rep 2017;7:43199. doi:10.1038/srep43199.
[25] Dai Y, Su W, Ding Z, Wang X, Mercanti F, Chen M, et al. Regulation of MSR-1 and CD36 in macrophages by LOX-1 mediated through PPAR-γ. Biochem Biophys Res Commun 2013;431:496–500. doi:10.1016/j.bbrc.2013.01.029.
[26] Metzger BE, Gabbe SG, Persson B, Buchanan TA, Catalano PA, Damm P, et al. International association of diabetes and pregnancy study groups recommendations on the diagnosis and classification of hyperglycemia in pregnancy. Diabetes Care 2010;33:676–82. doi:10.2337/dc09-1848.
[27] Chen X, Li P, Liu M, Zheng H, He Y, Chen MX, et al. Gut dysbiosis induces the development of pre-eclampsia through bacterial translocation. Gut 2020;69:513–22. doi:10.1136/gutjnl-2019-319101.
[28] Yang J, Wei H, Zhou Y, Szeto CH, Li C, Lin Y, et al. High-fat diet promotes colorectal tumorigenesis through modulating gut microbiota and metabolites. Gastroenterology 2022;162:135–49 e2. doi:10.1053/j.gastro.2021.08.041.
[29] Chen H, Tang X, Han TL, Zhu JN, Zhou W, Baker PN, et al. Potential role of FoxO3a in the regulation of trophoblast development and pregnancy complications. J Cell Mol Med 2021;25:4363–72. doi:10.1111/jcmm.16499.
[30] Smart K, Aggio R, Van Houtte J, Villas-Bôas S. Analytical platform for metabolome analysis of microbial cells using methyl chloroformate derivatization followed by gas chromatography-mass spectrometry. Nat Protoc 2010;5(10):170929. doi:10.1038/nprot.2010.108.
[31] Isomaa B, Almgren P, Tuomi T, Forsén B, Lahti K, Nissén M, et al. Cardiovascular morbidity and mortality associated with the metabolic syndrome. Diabetes Care 2001;24:683–9. doi:10.2337/diacare.24.4.683.
[32] Muzurović E, Mikhailidis DP, Mantzoros C. Non-alcoholic fatty liver disease, insulin resistance, metabolic syndrome and their association with vascular risk. Metabolism 2021;119:154770. doi:10.1016/j.metabol.2021.154770.
[33] Turnbaugh PJ, Ley RE, Hamady M, Fraser-Liggett CM, Knight R, Gordon JI. The human microbiome project. Nature 2007;449:804–10. doi:10.1038/nature06244.
[34] Bankole T, Winn H, Li Y. Dietary impacts on gestational diabetes: connection between gut microbiome and epigenetic mechanisms. Nutrients 2022;14(24):5269. doi:10.3390/nu14245269.
[35] Grigor'eva IN. Gallstone disease, obesity and the firmicutes/bacteroidetes ratio as a possible biomarker of gut dysbiosis. J Pers Med 2020;11(1):13. doi:10.3390/jpm11010013.
[36] Rizzardi KF, Indiani C, Mattos-Graner RO, de Sousa ET, Nobre-Dos-Santos M, Parisotto TM. Firmicutes levels in the mouth reflect the gut condition with respect to obesity and early childhood caries. Front Cell Infect Microbiol 2021;11:593734. doi:10.3389/fcimb.2021.593734.
[37] Da Silva CC, Monteil MA, Davis EM. Overweight and obesity in children are associated with an abundance of firmicutes and reduction of bifidobacterium in their gastrointestinal microbiota. Child Obes 2020;16:204–10. doi:10.1089/chi.2019.0280.
[38] Hasain Z, Mokhtar NM, Kamaruddin NA, Mohamed Ismail NA, Razalli NH, Gnanou JV, et al. Gut microbiota and gestational diabetes mellitus: a review

of host-gut microbiota interactions and their therapeutic potential. Front Cell Infect Microbiol 2020;10:188. doi:10.3389/fcimb.2020.00188.
[39] Virtue AT, McCright SJ, Wright JM, Jimenez MT, Mowel WK, Kotzin JJ, et al. The gut microbiota regulates white adipose tissue inflammation and obesity via a family of microRNAs. Sci Transl Med 2019;11(496):eaav1892. doi:10.1126/scitranslmed.aav1892.
[40] Nogal A, Valdes AM, Menni C. The role of short-chain fatty acids in the interplay between gut microbiota and diet in cardio-metabolic health. Gut Microbes 2021;13:1–24. doi:10.1080/19490976.2021.1897212.
[41] Nagata S, Chiba Y, Wang C, Yamashiro Y. The effects of the Lactobacillus casei strain on obesity in children: a pilot study. Benef Microbes 2017;8:535–43. doi:10.3920/bm2016.0170.
[42] Arora T, Sharma R. Fermentation potential of the gut microbiome: implications for energy homeostasis and weight management. Nutr Rev 2011;69:99–106. doi:10.1111/j.1753-4887.2010.00365.x.
[43] Russell WR, Hoyles L, Flint HJ, Dumas ME. Colonic bacterial metabolites and human health. Curr Opin Microbiol 2013;16:246–54. doi:10.1016/j.mib.2013.07.002.
[44] Larraufie P, Doré J, Lapaque N, Blottière HM. TLR ligands and butyrate increase Pyy expression through two distinct but inter-regulated pathways. Cell Microbiol 2017;19(2). doi:10.1111/cmi.12648.
[45] Kohan AB, Yoder SM, Tso P. Using the lymphatics to study nutrient absorption and the secretion of gastrointestinal hormones. Physiol Behav 2011;105:82–8. doi:10.1016/j.physbeh.2011.04.056.
[46] Taskinen MR, Björnson E, Kahri J, Söderlund S, Matikainen N, Porthan K, et al. Effects of evolocumab on the postprandial kinetics of Apo (Apolipoprotein) B100- and B48-containing lipoproteins in subjects with type 2 diabetes. Arterioscler Thromb Vasc Biol 2021;41:962–75. doi:10.1161/atvbaha.120.315446.
[47] Nauli AM, Nassir F, Zheng S, Yang Q, Lo CM, Vonlehmden SB, et al. CD36 is important for chylomicron formation and secretion and may mediate cholesterol uptake in the proximal intestine. Gastroenterology 2006;131:1197–207. doi:10.1053/j.gastro.2006.08.012.
[48] Lynes M, Narisawa S, Millán JL, Widmaier EP. Interactions between CD36 and global intestinal alkaline phosphatase in mouse small intestine and effects of high-fat diet. Am J Physiol Regul Integr Comp Physiol 2011;301:R1738–47. doi:10.1152/ajpregu.00235.2011.
[49] Plows JF, Stanley JL, Baker PN, Reynolds CM, Vickers MH. The pathophysiology of gestational diabetes mellitus. Int J Mol Sci 2018;19(11):3342. doi:10.3390/ijms19113342.
[50] Schreiber I, Dörpholz G, Ott CE, Kragesteen B, Schanze N, Lee CT, et al. BMPs as new insulin sensitizers: enhanced glucose uptake in mature 3T3-L1 adipocytes via PPARγ and GLUT4 upregulation. Sci Rep 2017;7:17192. doi:10.1038/s41598-017-17595-5.
[51] Meng Q, Qi X, Chao Y, Chen Q, Cheng P, Yu X, et al. IRS1/PI3K/AKT pathway signal involved in the regulation of glycolipid metabolic abnormalities by Mulberry (Morus alba L.) leaf extracts in 3T3-L1 adipocytes. Chin Med 2020;15:1. doi:10.1186/s13020-019-0281-6.
[52] Liu R, Chen Y, Liu G, Li C, Song Y, Cao Z, et al. PI3K/AKT pathway as a key link modulates the multidrug resistance of cancers. Cell Death Dis 2020;11:797. doi:10.1038/s41419-020-02998-6.